PCCP

The activation of carbon dioxide by first row transition metals (Sc – Zn)

Journal:	*Physical Chemistry Chemical Physics*
Manuscript ID	CP-ART-07-2018-004231.R2
Article Type:	Paper
Date Submitted by the Author:	13-Sep-2018
Complete List of Authors:	Blaziak, Kacper; University of Oslo, Department of Chemistry Tzeli, Demeter; National Hellenic Research Foundation, Theoretical and Physical Chemistry Institute Xantheas, Sotiris; Pacific Northwest National Laboratory, Physical Sciences Division Uggerud, Einar; University of Oslo, Department of Chemistry

PCCP

ARTICLE

The activation of carbon dioxide by first row transition metals (Sc – Zn)

Received 00th January 20xx,
Accepted 00th January 20xx

DOI: 10.1039/x0xx00000x

www.rsc.org/

Kacper Blaziak,[a,b] Demeter Tzeli,[c] Sotiris S. Xantheas[d,e] and Einar Uggerud[a,*]

The activation of CO_2 by chloride-tagged first-row transition metal anions $[ClM]^-$ (M=Sc-Zn), was examined by mass spectrometry, quantum chemical calculations, and statistical analysis. The direct formation of $[ClM(CO_2)]^-$ complexes was demonstrated in the reaction between $[ClM]^-$ and neutral CO_2. In addition, the reverse reaction was investigated by energy-variable collisionally induced dissociation (CID) of the corresponding $[ClM(CO_2)]^-$ anions generated in-source. Five different mono- and bi-dentate binding motifs present in the ion/CO_2 complexes were identified by quantum chemical calculations and the relative stability of the each of these isomers was established and analyzed for all first-row transition metals based on the experimental and theoretical ion/molecule binding energies. It was found that the early first row transition metals form strong covalent bonds with the neutral CO_2 molecule, while the late ones and in particular copper and zinc are weakly bonded. Using simple valence bond Lewis diagrams, the different binding motifs and their relative stabilities across the first row were described using multi-configurational self consistent field (MSCSCF) wavefunctions in a quantitative manner based on the electronic structure of the individual metals. This analysis provides an explanation for the change of the most favorite bonding motif of the transition metals with CO_2 along the 1st transition metal row. The nature of the activated CO_2 complex and the relationship between its stability and other structural and spectral properties was also analyzed by Principal Component Analysis (PCA) and Artificial Neural Networks.

I. Introduction

The discovery of new chemical procedures by which carbon dioxide can be activated, and thereby transformed to commodity chemicals in a thermodynamically controlled manner, is a challenging task but also an attractive outlook for the industry[1, 2] Any process in which carbon dioxide forms compounds with covalent C–C or C–H bonds is reductive by requiring input by electrons, as observed both in nature[3, 4] and electrochemical processes.[5, 6] Due to the fact that CO_2 has a negative electron affinity,[7] the presence of some auxiliary substrates – for example a transition metal or a solvent molecule[8-10]– are required for stabilizing one or two extra electrons. In any case, the reduction can proceed only when the CO_2 molecule is capable to actively coordinate to the metal core and take up electrons from either the metal catalyst or the metal-containing enzyme, after which the metal free CO_2^- anion can exist in a pure solvent enviroment.[8-30] In this respect, only partially negatively charged CO_2 can be considered an active chemical reagent, ready for chemical fixation. Over the years, much effort has been made to invent suitable methods, in which the CO_2 molecule would be catalytically converted into more complex molecular forms by metallic catalysts.[31-33] Besides the promising applied aspects of investigations of this sort, in order to fully understand how to control the reactivity of metal-CO_2 complexes, it is especially important to describe all essential physical properties, including complexation energies and structural differences in the coordination modes of the key metal carboxylate ionic species.

The mode of the CO_2 molecule coordination to the metal atom in the MCO_2 complexes depends on the size and charge state of the metallic core. Neutral complexes give mostly bidentate structures, (A) and (B) in Figure 1, respectively.[2, 34] The linear 'end-on' coordination (not shown above) is also possible for neutral systems but it is rare.[2] However, the linear mode ($^+$M-OCO), in which the partially negatively charged oxygen in CO_2 coordinates to the electron-deficient metal is the most common binding motif for cationic metal complexes.[35-41] During the last years, it has also been shown that some negatively charged transition and alkali metals may give rise to the (A) and (B) coordination motifs.[21, 23-26, 28-30, 42, 43]

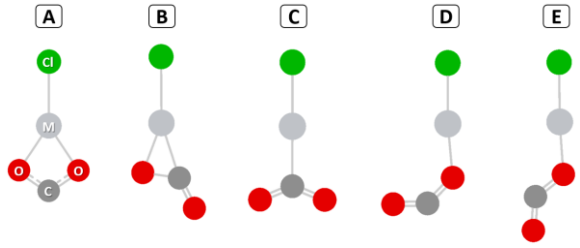

Figure 1. The $[ClM(CO_2)]^-$ coordination motifs (A) $ClM(\kappa^{2,O\text{-}O}\text{-}O_2C)$, (B) $ClM(\kappa^{2,C\text{-}O}\text{-}CO_2)$, (C) $ClM(\kappa^{1,C}\text{-}CO_2)$, (D) $ClM(\kappa^{1,O\alpha}\text{-}CO_2)$ and (E) $ClM(\kappa^{1,O\beta}\text{-}CO_2)$.

[a] Department of Chemistry and Hylleraas Centre for Quantum Molecular Sciences, University of Oslo, PO Box 1033, Blindern, Oslo N-0135, Norway Address here.
[b] Institute of Organic Chemistry, Polish Academy of Sciences, Kasprzaka 44/52, 01-224 Warsaw, Poland
[c] Theoretical and Physical Chemistry Institute, National Hellenic Research Foundation, 48 Vassileos Constantinou, Athens 116 35, Greece
[d] Advanced Computing, Mathematics and Data Division, Pacific Northwest National Laboratory, 902 Battelle Boulevard, P.O. Box 999, MS K1-83, WA, 99352, USA
[e] Department of Chemistry, University of Washington, Seattle, WA, 98195, USA
*Email: einar.uggerud@kjemi.uio.no
Electronic Supplementary Information (ESI) available:
See DOI: 10.1039/x0xx00000x

Nevertheless, the periodic trends and CO_2 capture abilities of different metal atoms have not been surveyed and analyzed in detail. In this respect, we present here an extensive mass spectrometric and theoretical chemical characterization of complexes of carbon dioxide bonded to first row transition metals tagged by a chloride anion, $[ClM(CO_2)]^-$. The differences in the CO_2 capture abilities between the various transition metal chloride anions will be discussed based on their theoretically computed and experimentally measured binding energies. Additional insight of the role of the activated CO_2 moiety in all of the isomeric forms of $[ClM(CO_2)]^-$ ions will be facilitated by quantum-chemical calculations yielding valence bond diagrams explaining the different bonding motifs assumed by the various metals, and Principal Component Analysis (PCA).

II. Experimental and computational details

Mass Spectrometry techniques. The gas phase experiments were conducted using two instruments: an API 3000 Triple-quadrupole (ABSciex, Framingham, MA, USA) and Q-TOF-2 (Waters Manchester, UK). Electrospray ionization (ESI) in the negative ion mode was applied in both cases to produce ClM^- and $[ClM(CO_2)]^-$ anions from mixtures of oxalic acid and metal (II) salts MCl_2 (M = Cr, Mn, Fe, Co, Ni, Cu, Zn) dissolved in methanol. The main $[ClM(CO_2)]^-$ and ClM^- ions were formed in two ways: upon collisional activation in the collision cell and in the ion source by the loss of one and two CO_2 molecules from oxalic acid metal complex $[ClM(CO_2)_2]^-$.[42, 44, 45] Accurate mass measurements and isotopic patterns confirm each of the ionic formulae. Collisionally induced dissociation (CID) experiments were performed for the $[ClM(CO_2)]^-$ ions using both instruments, where the Q-TOF-2 mass spectrometer was used for the experimental determination of the dissociation energies from the recorded breakdown curves (See SI). The bimolecular reaction spectra between the ClM^- ions and CO_2 were recorded using the API 3000 TQ Mass Spectrometer, which offers a higher collision efficiency by having a longer collision cell.

Quantum Chemical Calculations. All ground state structures of the $[ClM(CO_2)]^-$ complexes were optimized and the complexation energies were computed with six different DFT and *ab initio* methods using the aug-cc-pVTZ basis set (See SI). The potential energy surfaces of the $^1A_1$ and $^3B_2$ electronic states of neutral carbon dioxide as a function of the bond angle (∠OCO) were calculated at the CASSCF/aug-cc-pVDZ level of theory including 16 valence electrons in 12 active orbitals. No symmetry restrictions were used during the calculations. The number of configurations generated in the full valence space for the $^1A_1$ and $^3B_2$ electronic states were 18009 and 28376, respectively (35793 and 56592 under C_s symmetry). Additionally, the energies of neutral CO_2 moieties isolated from optimized $[ClM(CO_2)]^-$ complexes were computed at the CASSCF/aug-cc-pVDZ||CAM-B3LYP/aug-cc-pVTZ level with analogous active space restrictions. The neutral CO_2 and the anion CO_2^- were also calculated at the CCSD(T)/aug-cc-pVTZ level of theory. Finally, due to the inherently multireference character of the transition metals, CASSCF calculations were carried out for the $[ClM(CO_2)]^-$ complexes at the CASSCF/aug-cc-pVTZ||CAM-B3LYP/aug-cc-pVDZ level of theory in order to elucidate the bonding mechanisms of the clusters. The $1s^2 2s^2 2p^6 3s^2 3p^6$ (M), $1s^2 2s^2 2p^6$ (Cl) and $1s^2$ (C, O) electrons were kept frozen, twelve orbitals were forced to remain doubly occupied and three to thirteen "valence" (active) electrons were distributed between 10 orbitals. The CASSCF space ranges from 330 to 29700 configuration state functions (CSFs). The DFT calculations were performed using the Gaussian 09 Rev. D.01 suite of programs,[46] while the CASSCF calculations of the complexes were executed using the MOLPRO 2015.1 suite of codes.[47, 48] In addition, the neural network graphs presented in this study were constructed using the calculated correlation coefficients obtained by the Gephi 0.9.2 software.[49]

III. Results and discussion

Activation of CO_2: Mass-selected ClM^- ions were exposed to CO_2 in the collision cell of the mass spectrometer. All transition metal chloride anions (Cr, Mn, Fe, Co, Ni, Cu, Zn) that can be formed by ESI gave rise to signals corresponding to the various $[ClM(CO_2)]^-$ complexes (Figure 2) according to Eq. (1):

$$[ClM]^- + CO_2 \underset{\Delta E^\circ_{dissociation}}{\overset{\Delta E^\circ_{complexation}}{\rightleftharpoons}} [ClM(CO_2)]^- \qquad \text{Eq. 1}$$

The rather low abundance of the CO_2 adduct in all cases is related to the exothermic character of the process, since in order to form stable $[ClM(CO_2)]^-$ the hot short-lived collision complex must be stabilized by third body collisions. In the absence of stabilizing collisions, the hot complex will dissociate to reform the reactants. Under the conditions of this experiments, with a nominal CO_2 pressure of 3.5×10^{-3} mbar and collision energies around 1 eV, it is possible that complete equilibrium has not been reached. Consequently, the observed $[ClM(CO_2)]^-$ may include contributions from higher energy isomers in addition to the thermodynamically most stable complex.

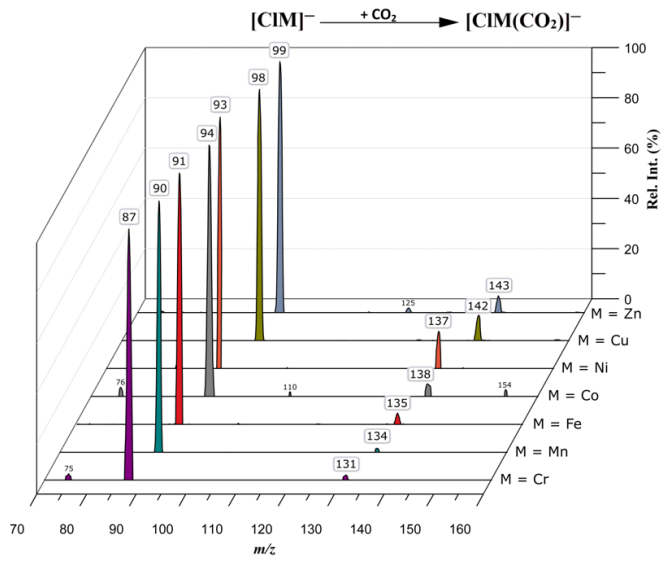

Figure 2. Mass spectra showing the $[ClM]^-$ + CO_2 reactions recorded at a nominal CO_2 pressure of 3.5 $\times10^{-3}$ mbar and a collision energy range of 0.47 – 1.29 eV (CM).

Since there is no clear relationship between the relative abundance of the product complexes and the stability of the most stable isomer in these experiments, separate experiments of the reverse reaction – dissociation of intact $[ClM(CO_2)]^-$ ions (Eq.1) – was examined experimentally in order to establish the reaction energies.

Deactivation of CO_2: Metal chloride carboxylates $[ClM(CO_2)]^-$ were introduced to the collision cell of the mass spectrometer, and CID experiments were performed. Fragment ion

mass spectra were recorded in steps in the interval 2–30 eV (laboratory frame) and the dissociation energies were determined from the recorded breakdown curves (Table 1).

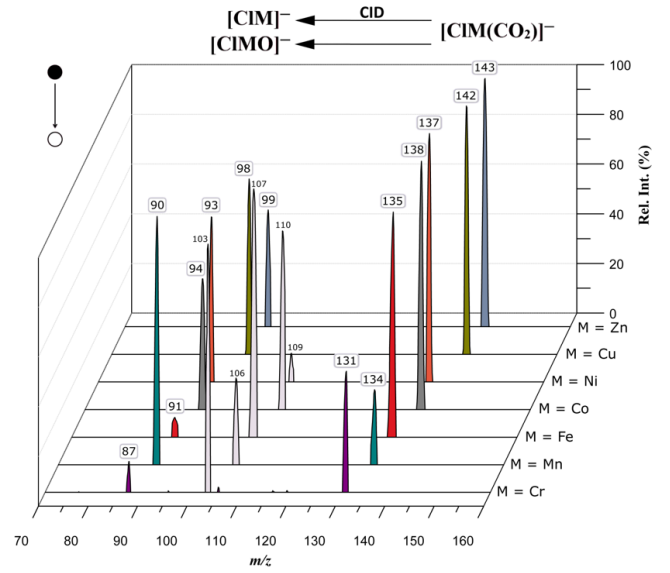

Figure 3. Fragmentation mass spectra of $[ClMCO_2]^-$ ions recorded at a collision energy range of 2.54–2.70 eV (CM) with nitrogen collision gas at a nominal pressure of 2.3 $\times 10^{-3}$ mbar.

Representative CID spectra for each of the $[ClM(CO_2)]^-$ ions, recorded with the triple-quadrupole mass spectrometer, are shown in Figure 3, while all recorded breakdown curves obtained using the Q-TOF mass spectrometer are given in the Supporting Information. Upon collisional activation, two main fragmentation channels were observed, corresponding to the loss of CO_2 and CO, respectively. For all metal-carboxylate complexes, the loss of CO_2 (deactivation of carbon dioxide) leads to $[ClM]^-$ ions. The second fragmentation pathway yielded $[ClMO]^-$ signals arising from the loss of a neutral CO molecule. The reduction of CO_2 to carbon monoxide by metal chloride anions was observed for M=Cr, Mn, Fe, and Co, but not for Zn and Cu. While highly interesting in its own right, only the former reaction channel will be analyzed here due to the complexity of the subject and the existence of already extensive amounts of data for this channel that are included in the present study (see SI). The CO loss reaction will be the subject of a future study.

Complexation Energies: Further insight into the observed phenomena was obtained through quantum chemical calculations. In particular, we applied several different levels of theory (based on both wavefunction and density functional theory) to explore the coordination sphere around the $[ClM]^-$ ions in an attempt to identify all possible isomeric forms of the CO_2 complexes. In general, all methods employed were were found to produce comparable energetic trends. We have chosen to highlight the results obtained with the CAM-B3LYP density functional, since it previously has been shown to accurately reproduce the molecular properties of metal-CO_2 complexes.[44] The complexation energies were computed across the entire first-row transition metal chloride carboxylates, including also scandium, titanium, and vanadium. The bidentate isomer (A) was found to be a local minimum on the potential energy surface for all transition metal complexes, except for Cu. A minimum for the bidentate (B) isomer was identified for the first eight transition metals (Sc-Ni) but not for Cu or Zn. The carbon-monodentate complex structure (C) $[ClM(\kappa^{1,C}\text{-}CO_2)]^-$ was found to exist only for the last two transition metals, namely Cu and Zn. Isomers where the metal is singly coordinated to one of the oxygen atoms in the CO_2 moiety were found for copper (D, E), nickel and cobalt (E). The computed complexation energies indicate that there is a clear periodic trend in the stability of the $[ClM(CO_2)]^-$ complexes (Figure 4). The $[ClSc]^-$ and $[ClTi]^-$ form the most stable complexes with CO_2, while along the first row of the transition metals the strength of ion-molecule interaction decreases progressively. A significant decrease is found for Mn, which is expected because all *d* orbitals are singly occupied and it does not form strong bonds from its ground state compared to other transition metals.[50, 51] The value of ΔE increases for Fe, Co, and Ni with the three of them having similar ΔE values, both computationally and experimentally. Finally, the ΔE values decrease significantly for Cu and even more for Zn due to the fact that both have fully occupied *d* orbitals and, in addition, in Zn also the 4*s* orbital is fully occupied.

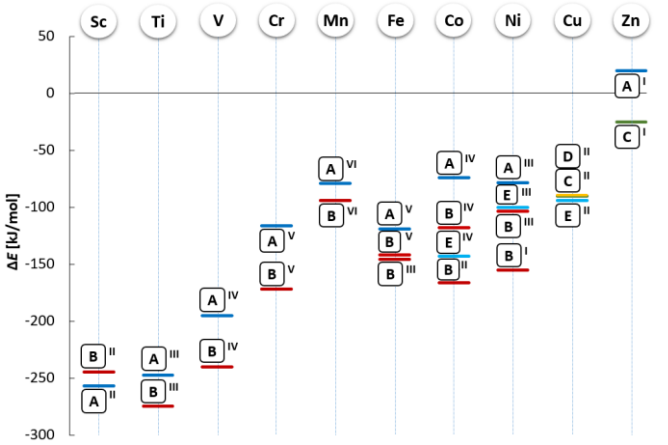

Figure 4. Complexation energies calculated with CAM-B3LYP/aug-cc-pVTZ level. The zero energy level corresponds to the infinitely separated reactants ($[ClM]^-$ + CO_2). Capital letters denote the coordination motifs shown in Figure 1 and Roman numerals indicate the multiplicity of the ionic structures.

Similar trends in the binding energies for the 3*d* transition metal have been reported for their oxides,[52] sulfides,[52] and borides.[50, 52] Bridgeman and Rothery have shown that the bond strength between the metal and the ligand can be inversely correlated with the atomic and ionic radii of the metal atoms and their ionization energies.[52] It should be noted that the calculated dissociation energies are in good agreement with the experimental ones, obtained from the recorded breakdown curves for Cr, Fe, Co, Ni, Cu, and Zn metal chlorides. It is known that DFT has difficulty in reproducing spin densities and dissociation energies accurately,[53, 54] however, in the case at hand it is found to perform quite well in this respect.

Structural Analysis of Bonding Motifs via Principal Component Analysis and Artificial Neural Networks: In order to qualitatively describe the essential structural differences between the $[ClM(CO_2)]^-$ geometries and other properties, the full set of the complexes shown in Figure 4 was analyzed by principal component analysis (PCA). Altogether, 14 variables describing 26 different $[ClM(CO_2)]^-$ structures were taken into account during the statistical analysis (see section 3 in the SI). All bond distances and valence angles, four main vibrational frequencies ($\nu_{1\text{-}4}$) related to the carbon dioxide moiety, the partial charge of the CO_2 moiety $\delta^-(CO_2)$, and the relative binding energies (ΔE) of the $[ClM(CO_2)]^-$ complexes were used as descriptors.

Table 1. Complexation energies ΔE [kJ/mol] for the various metals and bonding motifs of Figure 1.

Isomer	Sc ^{II}	Ti ^{III}	V ^{IV}	Cr ^{V}	Mn ^{VI}	Fe	Co	Ni	Cu ^{II}	Zn ^{I}
A	−257	−247	−195	−116	−79	−119 ^{V}	−74 ^{IV}	−78 ^{III}	-	20
B	−244	−275	−240	−172	−94	−145 ^{III} −142 ^{V}	−166 ^{II} −143 ^{IV}	−155 ^{I} −103 ^{III}	-	-
C	-	-	-	-	-	-	-	-	−90	−25
D	-	-	-	-	-	-	-	-	−89	-
E	-	-	-	-	-	-	−118 ^{IV}	−100 ^{III}	−94	-
Exp.	-	-	-	−163 (±66)	−80 (±32)	−120 (±48)	−124 (±50)	−137 (±55)	−60 (±24)	−25 (±10)

$\Delta E = E[\mathrm{ClM(CO_2)^-}] - (E[\mathrm{ClM^-}] + E[\mathrm{CO_2}])$. Numbers include zero-point energy corrections. Isomers (A) – (E) refer to the coordination motifs presented in Figure 1 and Roman numerals indicate the multiplicity of the ionic structures.

The complete results of the PCA are presented in the SI, while the essential score plot is shown in Figure 5. The analysis suggests that about 45% of the total variation is explained by the first principal component (PC1), 70% by the first two PCs, and 82% by the first three principal components. The most important variables for PC1 are the three geometry parameters [∠OCO, d(C-O^2), d(O^1-O^2)], the partial charge of the CO_2 moiety $\delta^-(CO_2)$, and one vibrational frequency [$\nu_3^{\mathrm{antisym}}(CO_2)$]. The second principal component PC2 contains the relative binding energies (ΔE), two geometrical parameters [d(C-O^1), d(M-Cl)] and two vibrational frequencies [$\nu_2^{\mathrm{sym}}(CO_2)$, ν_4(M-CO_2)].

The score plot (Figure 5) computed on the basis of information from all isomers shows the location of the objects ([ClM$(CO_2)]^-$ complexes) in the multivariate space of the two first principal component score vectors. It can be seen that the scores are arranged in four distinct groups. The first one includes all (A)-type isomers, the second one all (B) structures, and the third contains only two (C)-type isomers containing copper and zinc metal atoms. The fourth group consists of (D) and (E) isomers, in both of which the metal core is singly bonded to one of the oxygen atoms in the CO_2 molecule. In addition, an essentially diagonal separation was observed between the complexes in which the metal cores are bonded only with oxygen atoms (A, D, E) and those where the metal core strongly interacts with the carbon atom (B, C).

In order to further analyze the relationship between the stability of the complexes and other physical factors, an artificial neural network (ANN) was constructed based on calculated Pearson's[55] correlation coefficients (ρ) between the 14 variables describing the full set of 26 structures including all (A-E) isomers, (A) and (B) isomers separately. (For more details see SI)

The neural network analysis shows that there is no strong overall linear, two-dimensional relationship between the energy of complexation (ΔE) and any other single variable. On the other hand, a multidimensional relationship between a number of structural and spectral factors and the ΔE values was found.

However, several important correlations were found for the (B)-type isomers. Significant positive correlations were found between ΔE and the symmetric stretch of the CO_2 moiety (ρ=0.8)

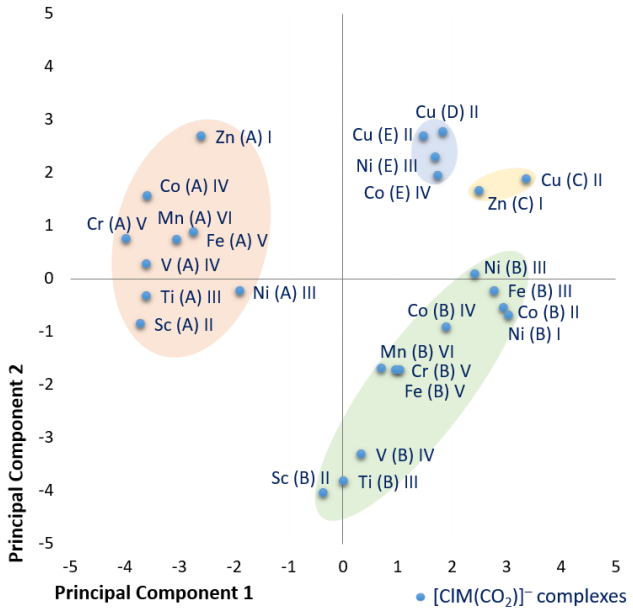

Figure 5. Score plot obtained by Principal Component Analysis. PC1 and PC2 account for 45% and 25% of the variance, respectively.

and the ∠OCO (ρ=0.6), ∠MCO^1 (ρ=0.7) valence angles. In addition, four negative correlations between the ΔE of the (B)-type isomers and d(C-O^1) (ρ=−0.7), d(M-Cl) (ρ=−0.7), ∠MCO^1 (ρ=−0.6), ν_4(M-CO_2) (ρ=−0.6) were identified.

The theoretically predicted periodic trend and relationships between the relative stability of the [ClM$(CO_2)]^-$ ions and the vibrational and geometric parameters of the CO_2 ligand can be related to the infrared spectroscopy measurements of the first-row transition metal-CO_2 cluster ions $[M(CO_2)_{2\text{-}8}]^-$, published in a series of papers by Weber and co-workers[24-26, 29, 30].

The authors have presented photodissociation action spectra recorded for $[M(CO_2)_3]^-$ ions with characteristic spectral features between 1600−1900 cm^{-1}. The main IR peaks correspond to the antisymmetric stretches of two CO_2 molecules bonded to the metal

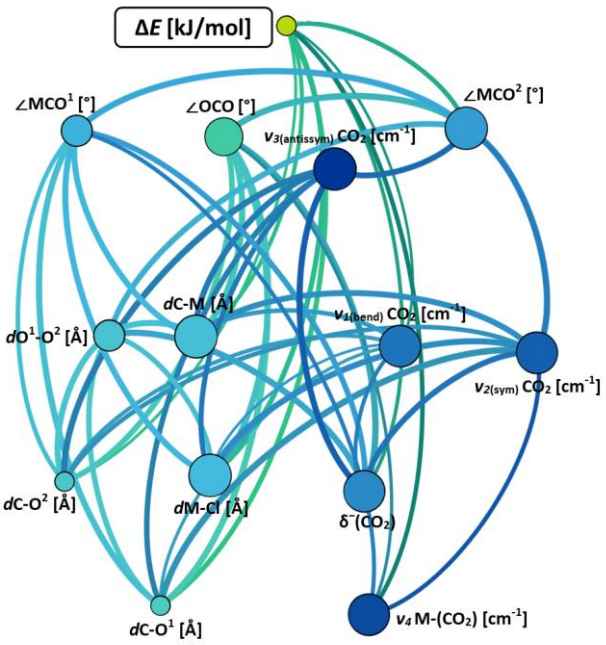

Figure 6. Artificial neural network of negative correlations, constructed based on the calculated Pearson's correlation coefficients between 14 variables for eleven B isomers. Note that different shades of the principal blue colour were introduced just to enhance visibility and they do not indicate the strength of the connections.

core in a "butterfly" mode, where both CO_2 molecules coordinate to the metal atom in a (B)-type motif. The key spectral features recorded for manganese containing[29] cluster ions were located at 1680 and 1724 cm^{-1}, for iron[30] at 1699 and 1749 cm^{-1}, and for cobalt[26] at ~1750 and ~1780 cm^{-1}. Nickel[25] and copper[24] core–CO_2 clusters were characterized by three spectral features corresponding to overlapping antisymmetric CO_2 stretches of two very similar cluster isomers at ~1740; ~1770 and ~1790 cm^{-1} and at ~1750; ~1780 and ~1820 cm^{-1}, respectively. It can be seen that the experimentally measured band origins of the main features are clearly red-shifted in the periodic trend Mn < Fe < Co < Ni < Cu. Furthermore, these authors have suggested that the observed red shift of the antisymmetric stretches of asymmetric (B)-like isomers can be correlated to the amount of negative charge deposited on the partially reduced CO_2 moiety.[22, 23, 30]

It can be seen in the presented connection network constructed for (B)-type isomers (Figure 6, right) that the partial charges of the CO_2 ligand in (B)-type isomers are strongly negatively correlated with the symmetric (ρ=−0.9) and antisymmetric CO_2 stretches (ρ=−0.85). Additionally, a large linear correlation coefficient (R^2=0.87) was found between $\delta^-(CO_2)$ and the latter variable (see S87), showing that highly negatively charged CO_2 moieties result in lower antisymmetric vibrational frequencies. The extent of the experimentally observed red shifts[22-26, 29, 30] strongly supports the proposed trend derived from the statistical analysis and the computed CO_2 partial charges.

In situ Electronic Structure of Activated CO_2 in the Metal Complexes: In order to obtain additional insight into the in situ electronic structure of the activated CO_2 moieties in the $[ClM(CO_2)]^-$ complexes, potential energy surfaces (PES) for the neutral carbon dioxide molecule for the singlet ($^1A_1$) and triplet ($^3B_2$) electronic states were computed as a function of the ∠OCO bond angle (Figure 7).

The left panel of Figure 7 shows the energies of gas phase CO_2 as a function of the OCO angle, in which for each individual OCO angle the C-O bond lengths were optimized on both the singlet ($^1A_1$) and triplet ($^3B_2$) PESs under C_{2v} symmetry. Two minima were identified on the $^1A_1$ state PES, corresponding to the linear (global minimum, ∠OCO = 180º) and bent (local minimum, ∠OCO = 73.5º) CO_2 molecule. The minimum on the $^3B_2$ state PES was located for ∠OCO = 118.2º. The computed geometries and relative energies correctly reproduce the results reported previously by Xantheas[56-58] and Yu.[59] The higher lying minimum at smaller bond angles originates from the interaction between states of the same symmetry as previously discussed for this and other triatomic molecules.[56, 60] Moreover, an approximate interpolation of the two intersecting PESs was performed in order to estimate the location of two spin crossover points (SCO) between the $^1A_1 \rightarrow {}^3B_2$ and $^3B_2 \rightarrow {}^1A_1$ electronic states. The SCO(1) and SCO(2) points correspond to the CO_2 structures with ∠OCO = 88.1º and 105.1º, respectively (See S82-S83).

The right panel of Figure 7 shows the single point CASSCF/aug-cc-pVDZ energies for all activated CO_2 moieties taken as neutral molecules at their geometries in the optimized $[ClM(CO_2)]$─ complexes (Figure 4) for the $^1A_1$ and $^3B_2$ electronic states. The coordinate area indicated by the rectangular frame on the left panel in Figure 7 was magnified and the energies of the appropriate "frozen" CO_2 moieties were plotted on the right panel of Figure 7. The range of ∠OCO valence angle for all calculated metal-CO_2 complexes lies between 108.39 – 139.20 degrees. Note that the energies of the neutral CO_2 in the corresponding geometries of the complexes (blue and red dots in the right panel of Figure 7) are above the solid line curves, which correspond to the energies of the gas phase optimized CO_2 structures for each OCO angle. The carbon dioxide moiety became most bent when activated in the form of the (A)-type isomers. It can be seen that the energies of the CO_2 moieties for the (A)-type complexes in the $^1A_1$ and $^3B_2$ electronic states, respectively, are very close to each other and lie close to the spin state crossover point SCO(2) spanning a range of ca. 107º < OCO < 115º. The possible mixed singlet-triplet electronic character of the CO_2 moiety and the geometry of the carbene-like carbon atom in the $[ClM(\kappa^{2,O-O}\text{-}O_2C)]^-$ structures suggests that this particular isomeric form should be the most reactive for the case of the CO_2 fixation processes. This conclusion, derived from the presented calculations, has recently been corroborated in a recent paper by Miller and Uggerud.[44] These authors presented an extensive theoretical and experimental study on the reactivity of magnesium and zinc (A)-type $[ClM(CO_2)]^-$ complexes with acetaldehyde, and reported a new C-C bond formation between the metal-activated CO_2 and a neutral molecule, leading to the formation of the pyruvate ionic species. For the other kinds of complexes (B)-(E), the carbon dioxide molecule is also significantly bent (OCO angle in the range 123 – 140º) but less than in the (A)-type structures. The differences in the calculated energies for the $^1A_1$ and $^3B_2$ electronic states of the CO_2 moieties in the (B)-(E) isomers suggest that in these structures the incipient electronic state of the CO_2 moieties is most likely that of a singlet.

Analysis of Bonding Motifs of Various Metals via Valence Bond Lewis Diagrams: Our calculations indicate that in free $[MCl]^-$ anions the bonding is due to the interaction between the anion Cl^- (^1S) state and the ground state of metal Sc(^2D), Ti(^3F), V(^4F), Cr(^7S), Mn(^6S), Fe(^5D), Co(^4F), Ni(^3F), Cu(^2S), and Zn(^1S) states. This is in agreement with previous calculations on $[ScCl]^-$, $[TiCl]^-$, $[VCl]^-$, $[CrCl]^-$,[61] and $[FeCl]^-$[62] and similar ones for the case of metal diatomic fluoride anions, MF^-.[7, 61-65]

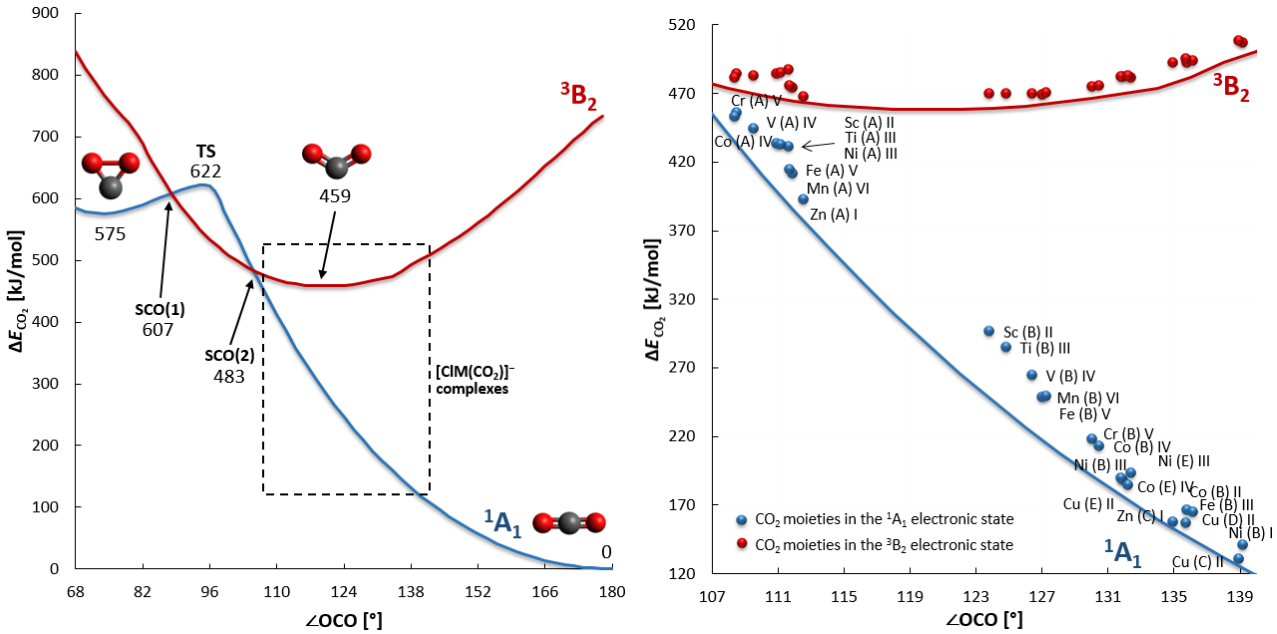

Figure 7. Potential energy surfaces of the $^1A_1$ and $^3B_2$ states along the bending coordinate of symmetric CO_2 (C_{2v}). Calculations were performed at the CASSCF/aug-cc-pVDZ level of theory including 16 electrons in 12 valence orbitals. The coordinate area indicated by the rectangular frame on the left was magnified and is shown on the right-hand side. The energies of the $^1A_1$ (blue) and $^3B_2$ (red) electronic states of CO_2 moieties taken as neutral from all $[ClM(CO_2)]^-$ complexes are shown on the right-hand side.

At first, we analyze the possible bonding motifs that neutral CO_2 and anionic CO_2^- can form with metal atoms. The CO_2 molecule is linear with carbon forming two double bonds with the two oxygen atoms. As the molecule bends, the double bond character of the C=O bonds diminishes. Using a valence bond description, this results in a situation for both the $^3B_2$ and in the $^1A_1$ states, where spin density develops on both the C and O atoms, Scheme 1. The two electrons of each valence bond representation have parallel spins in the triplet state and anti-parallel ones in the singlet state. Thus, the C and O atoms of CO_2 can form two bonds with M (B bonding motif), or only one bond with M either from C or O (C, D or E bonding motifs), see Scheme 1. The last scenario (C, D, or E motifs) should be less stable than B because only one bond is formed. CO_2 has a negative electron affinity calculated at 39.2 and 60.9 kJ/mol at the CAM-B3LYP/aug-cc-pVTZ and CCSD(T)/aug-cc-pVTZ levels of theory, respectively. The CCSD(T) result is in agreement with the experimental value of 58±19 kJ/mol.[7] Despite its negative electron affinity, CO_2 is capable of actively coordinating to the metal core and take up electrons from the metal/ligand. The CO_2^- anion has an additional electron delocalized in the O atoms and a single electron on C atom, see Scheme 1. Thus, the CO_2^- anion can form: (*i*) a single σ bond between C and the metal (C bonding motif), (*ii*) a bond between C and M and an additional bond between O^- and M (B bonding motif), (*iii*) a bond between O^- and M (D and E bonding motifs), and finally (*iv*) the two O atoms can each donate electrons back to M, thus forming two bonds (A bonding motif). As it can be seen from Figure 7, the distorted CO_2 in the examined complexes lies from 130 – 450 kJ/mol above the ground state of CO_2. However, electron transfer from MCl^- to CO_2 reduces significantly the energy difference to ~60 kJ/mol. Therefore, CO_2 and Cl are negatively charged while the metals are positively charged in the above complexes.

For all complexes having the A bonding motif, a charge of about 1.3 e^- is transferred to CO_2. The C-O bond distances are about 1.32 Å and the ∠OCO angle is about 110°, compared to 1.225 Å and 137.6° in the isolated CO_2^-. Therefore, the ∠OCO angle is smaller, and the C-O bond distances are elongated in the complexes with respect to the isolated CO_2, so both O atoms can interact efficiently with M. This is the reason why the CO_2 moiety becomes the most bent when it is activated in the form of the A-type isomers. In contrast, in the C bonding motif, where the only interaction is between C and M, the corresponding values are 1.22 Å and 137°, viz. similar to the isolated CO_2^- (see SI). In the B bonding motif, the C-O bond distances are ~1.30 – 1.37 Å and 1.21 Å and the ∠OCO angle is ~125°. These values are similar to those found in the HCOOH molecule, namely 1.338 Å, 1.194 Å, and 124.8°. Therefore, in this bonding motif (B) we have essentially one C=O double and one C–O single bond. Finally, in the E and D bonding motifs the C–O bond distances are ~ 1.27 Å and 1.20 Å, indicating that there is a double bond and another one stronger than a single bond given that the typical bond distances of a single and a double bond are about 1.34 Å and 1.19 Å, respectively. Consequently, the CO_2 moieties in the (B) – (E) isomers correspond to open shell states.

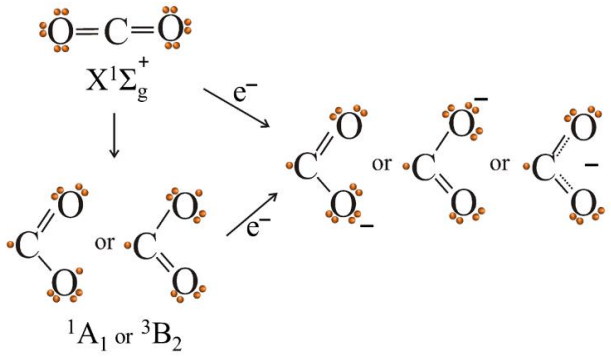

Scheme 1. Valence bond Lewis diagrams for neutral and negatively charged CO_2 molecules.

The molecular orbitals (MOs) obtained from the CASSCF calculations and the corresponding population analysis are instructive in revealing the bonding inside the complexes, see SI. Below we describe the bonds via valence bond Lewis representations. Cl is negatively charged, and its interaction with metal atoms has a significant electrostatic character. About 0.25 e^- is transferred from Cl^- via the metal to CO_2, while M is positively charged with charges ranging from +0.3 to +1.3 e^-. The C atoms obtain a negative charge only in the A bonding motif. For all metals, we observe extensive (4*s*4*p*) hybridization, in which between 0.1 and 0.5 e^- is transferred from the 4*s* to the 4*p* orbitals.

In the case of the $[ClSc(CO_2)]^-$, $[ClTi(CO_2)]^-$, $[ClV(CO_2)]^-$, $[ClCr(CO_2)]^-$ and $[ClMn(CO_2)]^-$ complexes, the lowest energy structures correspond to the A and B bonding motifs, see Scheme 2. It should be noted that for all five metals, significant (*sd*) hybridization is observed with electron transfer from one of the *d* orbitals to the 4*s* orbital for both motifs. In the A motif there is a bond between the 4*s* orbital of the metal towards the CO_2 molecule resulting in a transfer of about 1.3 e^-, with back bonding from the *p* orbitals of the O to the *d* orbitals of the metal. In the B motif, the character of the activated bond changes from C=O to C–O one electron is transferred from C to O. Then, electron density of the originally doubly occupied 4*s* of M forms a bond with the originally positively charged C, upon which 0.8 e^- is transferred. Back bonding is established between the O atom to the *d* orbitals of M. In the case of Sc, the A motif is more strongly bonded than B because only one *d* orbital is occupied, while in the other four the *d* orbitals start being partially occupied. Thus, for the remaining four metals the B motif is the more stable. It should be noted that the bond between CO_2 and Sc, Ti, V, and Mn, respectively, is formed from the respective ground states, $s^2d^{1\text{-}5}$. For Cr the bond is formed from the exited s^2d^4 atomic state, which lies 93 kJ/mol above the ground s^1d^5 state. This explains why both the calculated and experimental complexation energies of Cr (-172 and -163±66 kJ/mol, respectively for the B-type and -116 kJ/mol for the A-type) are significant smaller than those of Sc, Ti and V (about 80 kJ/mol smaller than the corresponding values for V). Additionally, the finding that Mn has the most elongated M–C and M–O bonds of all other ten metals is consistent with the fact that Mn has all its *d* orbitals singly occupied and for this reason does not form strong bonds from its ground state compared to other transition metals.[50, 51] The complexation energies for both the A and B motifs of Mn are indeed significantly smaller than the corresponding values of the previous four metals; for instance, the complexation values for Mn are about one third of the values of those for the complexes of Sc.

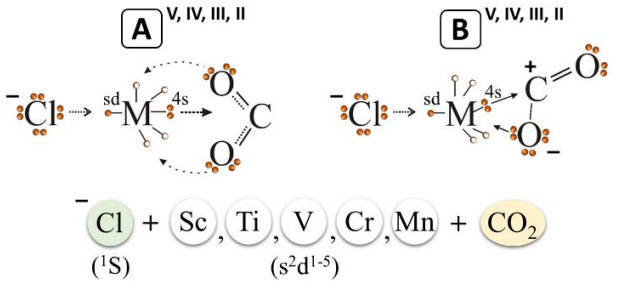

Scheme 2. Valence bond Lewis diagrams for $[ClM(CO_2)]^-$ containing Sc-Mn metal atoms.

In the case of the $[ClFe(CO_2)]^-$, $[ClCo(CO_2)]^-$, and $[ClNi(CO_2)]^-$ complexes the two lowest energy structures correspond to the B bonding motifs with different spin multiplicity, see Scheme 3. In both cases two bonds are formed between the M and the C and O atoms. It should be noted that (*sd*) hybridization is observed between one of the *d* orbitals and the 4*s* orbital. In the A motif, there is only one bond between the sd^2 orbital of the metal towards the CO_2 molecule. Finally, in the E bonding motif a single C-O bond is formed, and one electron is located on the C atom.

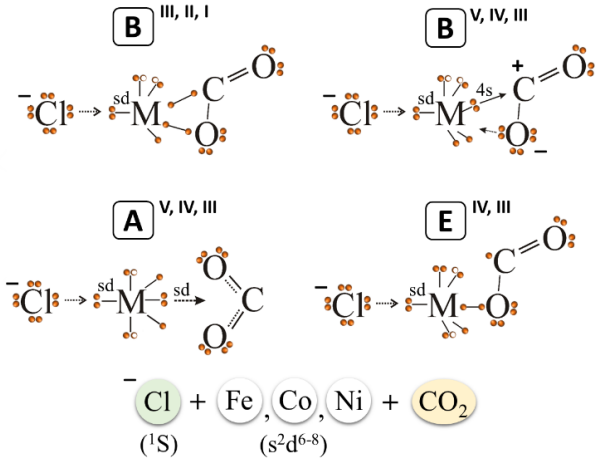

Scheme 3. Valence bond Lewis diagrams for $[ClM(CO_2)]^-$ containing Fe-Ni metal atoms.

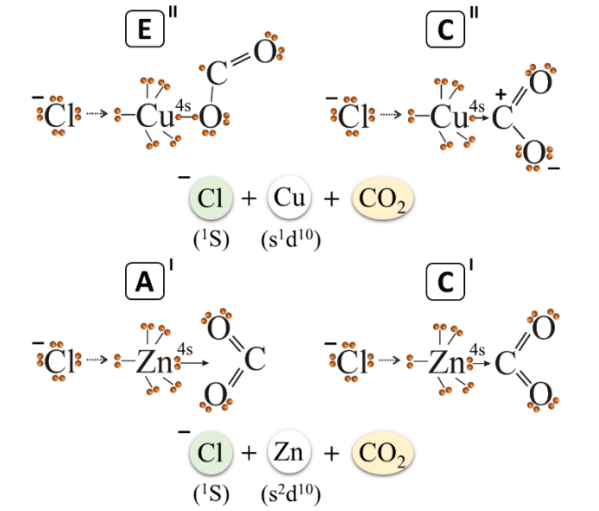

Scheme 4. Valence bond Lewis diagrams for $[ClM(CO_2)]^-$ containing Cu and Zn metal atoms.

In the $[ClCu(CO_2)]^-$ complex, the C=O bond has been partially broken in the E and D bonding motifs, see Scheme 4. The 4*s* electron of Cu forms a bond with a *p* orbital of the O atom, while a single electron is found in a *sp* orbital of C. Cu prefers to form a single bond with the O rather than with the C atom because the bond is stronger. In the C bonding motif, one electron of carbon has been transferred to O and a half bond is formed from the $4s^1$ orbital of Cu to the C atom. In contrast, for the $[ClZn(CO_2)]^-$ complex the C bonding motif is the most stable because in Zn all 3*d* and 4*s* orbitals are occupied and as such it prefers to interact mainly by dative bonding to C^+ see Scheme 4. In the A bonding motif, Zn has lost 1 e^-. Zn^+ interacts electrostatically with CO_2 via the O atoms, but Zn^+ is not as stable as Zn and the whole bonding motif is destabilized. It should be noted that the reduction of CO_2

to CO is not favorable for Zn and Cu because in these metals all the 3*d* orbitals are fully occupied and they do not prefer to form $[ClMO]^-$

It appears rational that for the complex of Sc, where Sc has only one *d* electron, the A bonding motif will be the most favorable, so as three strong bonds can be formed. Then, along the 1st transition metal row the B bonding motif, where the π component of the double C=O bond breaks upon which two single bonds are formed between the C and O atoms and the metal, is the favorite one up to Ni. Cu which has occupied fully all its *d* orbitals prefers to form only a single bond via the $4s^1$ orbital with the O of CO_2 resulting in the E bonding motif being the most favorable. Finally, Zn which has all its 4*s*3*d* orbitals occupied, prefers dative bonding and the C-type is the most favorable because the C atom is the only positively charged atom of CO_2.

IV. Conclusions

It is shown that chloride-tagged transition metal anions $[ClM]^-$ (M=Sc-Zn) are capable of capturing a carbon dioxide molecule and activating it via a significant bending of the ∠OCO angle in the range of 108 – 139º. A periodic trend in the stability of the $[ClM(CO_2)]^-$ complexes derived from quantum chemical calculations and experimental CID measurements shows that the early first-row transition metals form the most stable ion/CO_2 structures while Cu and Zn are weakly bonded to the CO_2 molecule. The particular bonding motif that each metal prefers is explained using valence bond Lewis diagrams that describe the origin and nature of the bond. Depending on the size of the metal core and mainly on the number of its *d* electrons, five different binding motifs for the $[ClM(CO_2)]^-$ complexes were found. A bidentate, A-type motif was identified for nine transition metals (Sc-Ni and Zn) and another isomer (B), in which the metal coordinates with both C and O atoms, for the first eight (Sc-Ni) metal cores. Monodentate, oxygen-bonded forms were found for Ni (E-type isomer) and Cu (E- and D-type isomers), while a single carbon-bonded C-type motif was located for the last two transition metals, Cu and Zn (cf. Figure 1). The A-type motif is preferred for Sc because it has four empty *d* orbitals. Moving along the 1st transition metal row up to Ni, it is seen that the B-type motif is preferred, in which the π component of the double C=O bond breaks upon which two single bonds are formed between the metal and C and O atoms. Since all *d* electrons are paired in Cu, the E-type motif is preferred, giving rise to only one single bond with one of the O atoms of CO_2. Finally, Zn prefers dative bonding (C-type) because all its 4*s*3*d* orbitals are occupied and the C atom is the only positively charged atom of the CO_2 moiety.

Structural analysis supported by principal component analysis (PCA) revealed a substantial grouping of the isomers in four basic bonding motifs. Additionally, the essential separation of oxophilic- and carbophilic-like isomers was clearly shown by the first two principal components, related to the relative stability of the complexes, the partial charge of the CO_2 moiety and the CO_2 vibrational frequencies. Moreover, the calculated correlation coefficients between 14 variables describing the geometry and spectral properties of the examined ion-CO_2 complexes showed several important correlations between the relative stabilities and other factors. A direct positive correlation between the complexation energy (ΔE) and the symmetric vibrational stretches of the CO_2 moiety was found for the full set of isomers, while a strong negative correlation between the symmetric and antisymmetric stretches, and the partial charge of CO_2 moieties in the bidentate B-type complexes was observed, indicating that the frequencies for the more negatively charged CO_2 moieties are correspondingly more red-shifted. Finally, the energy distribution of the activated CO_2 moieties in the $[ClM(CO_2)]^-$ geometries in their singlet and triplet electronic states indicates that the A-type isomers potentially constitute the most reactive forms of activated carbon dioxide among the examined series because the bonding has strong ionic character, while in the B-type isomers two covalent bonds are formed. The above results thus provide a consistent understanding at the molecular level of the selectivity and corresponding structural motifs of the various first row transition metals in activating CO_2.

Author information

Corresponding Author

*Email: einar.uggerud@kjemi.uio.no

Author Contributions

Kacper Blaziak conducted all experiments and data analysis, performed most quantum chemical calculations, conducted the statistical analysis and wrote the manuscript. Demeter Tzeli performed quantum chemical calculations, conducted the analysis of bonding motifs of various metals via valence bond Lewis Diagrams and contributed to the manuscript. Sotiris S. Xantheas provided key ideas, designed and performed quantum chemical calculations, performed analysis and wrote the manuscript. Einar Uggerud designed and supervised the study and wrote the manuscript.

Conflicts of interest

There are no conflicts to declare

Acknowledgements

This work was supported by the Norwegian Research Council through Grant No. 249788, The chemistry of CO_2 activation and fixation; to the Hylleraas Centre for Quantum Molecular Sciences No. 262695/F50 through their Centre of Excellence program, and the Norwegian Supercomputing Program (NOTUR) through a grant of computer time (Grant No. NN4654K). SSX acknowledges support from the Center for Scalable Predictive methods for Excitations and Correlated phenomena (SPEC), which is funded by the U.S. Department of Energy, Office of Science, Basic Energy Sciences, Chemical Sciences, Geosciences and Biosciences Division, as part of the Computational Chemical Sciences Program at Pacific Northwest National Laboratory. Battelle operates the Pacific Northwest National Laboratory for the U.S. Department of Energy. This research also used computer resources provided by the National Energy Research Scientific Computing Center, which is supported by the Office of Science of the U.S. Department of Energy under Contract No. DE-AC02-05CH11231. The authors are indebted to Prof. Witold Danikiewicz for providing access to the mass spectrometry facility at Institute of Organic Chemistry, Polish Academy of Sciences, and for scientific advice.

Notes and references

1. M. Aresta and A. Dibenedetto, *Dalton Trans.*, 2007, DOI: 10.1039/B700658F, 2975-2992.

2. M. Cokoja, C. Bruckmeier, B. Rieger, W. A. Herrmann and F. E. Kühn, *Angew. Chem. Int. Ed.*, 2011, **50**, 8510-8537.
3. R. J. Ellis, *Trends Biochem. Sci.*, 1979, **4**, 241-244.
4. M. B. Bishop and C. B. Bishop, *J. Chem. Educ.*, 1987, **64**, 302.
5. M. Tokuda, *J. Nat. Gas Chem.*, 2006, **15**, 275-281.
6. I. Ganesh, *Renew. Sust. Energ. Rev.*, 2016, **59**, 1269-1297.
7. R. N. Compton, P. W. Reinhardt and C. D. Cooper, *J. Chem. Phys.*, 1975, **63**, 3821-3827.
8. C. E. Klots and R. N. Compton, *J. Chem. Phys.*, 1979, **71**, 4172-4172.
9. C. E. Klots and R. N. Compton, *J. Chem. Phys.*, 1978, **69**, 1636.
10. C. E. Klots and R. N. Compton, *J. Chem. Phys.*, 1977, **67**, 1779-1780.
11. T. Habteyes, L. Velarde and A. Sanov, *Chem. Phys. Lett.*, 2006, **424**, 268-272.
12. T. Habteyes, L. Velarde and A. Sanov, *J. Chem. Phys.*, 2007, **126**, 154301.
13. E. Surber, R. Mabbs, T. Habteyes and A. Sanov, *J. Phys. Chem. A*, 2005, **109**, 4452-4458.
14. T.-W. Lam, H. Zhang and C.-K. Siu, *J. Phys. Chem. A*, 2015, **119**, 2780-2792.
15. R. F. Höckendorf, C.-K. Siu, C. van der Linde, O. P. Balaj and M. K. Beyer, *Angew. Chem. Int. Ed.*, 2010, **49**, 8257-8259.
16. C. van der Linde, A. Akhgarnusch, C.-K. Siu and M. K. Beyer, *J. Phys. Chem. A*, 2011, **115**, 10174-10180.
17. R. F. Höckendorf, Q. Hao, Z. Sun, B. S. Fox-Beyer, Y. Cao, O. P. Balaj, V. E. Bondybey, C.-K. Siu and M. K. Beyer, *J. Phys. Chem. A*, 2012, **116**, 3824-3835.
18. A. Akhgarnusch, R. F. Höckendorf, Q. Hao, K. P. Jäger, C.-K. Siu and M. K. Beyer, *Angew. Chem. Int. Ed.*, 2013, **52**, 9327-9330.
19. C. van der Linde, S. Hemmann, R. F. Höckendorf, O. P. Balaj and M. K. Beyer, *J. Phys. Chem. A*, 2013, **117**, 1011-1020.
20. A. Akhgarnusch, W. K. Tang, H. Zhang, C.-K. Siu and M. K. Beyer, *Phys. Chem. Chem. Phys.*, 2016, **18**, 23528-23537.
21. A. D. Boese, H. Schneider, A. N. Glöß and J. M. Weber, *J. Chem. Phys.*, 2005, **122**, 154301.
22. B. J. Knurr and J. M. Weber, *J. Am. Chem. Soc.*, 2012, **134**, 18804-18808.
23. B. J. Knurr and J. M. Weber, *J. Phys. Chem. A*, 2013, **117**, 10764-10771.
24. B. J. Knurr and J. M. Weber, *J. Phys. Chem. A*, 2014, **118**, 10246-10251.
25. B. J. Knurr and J. M. Weber, *J. Phys. Chem. A*, 2014, **118**, 8753-8757.
26. B. J. Knurr and J. M. Weber, *The Journal of Physical Chemistry A*, 2014, **118**, 4056-4062.
27. B. J. Knurr and J. M. Weber, *J. Phys. Chem. A*, 2015, **119**, 843-850.
28. M. C. Thompson and J. M. Weber, *Chem. Phys. Lett.*, 2017, **683**, 586-590.
29. M. C. Thompson, J. Ramsay and J. M. Weber, *J. Phys. Chem. A*, 2017, **121**, 7534-7542.
30. M. C. Thompson, L. G. Dodson and J. M. Weber, *J. Phys. Chem. A*, 2017, **121**, 4132-4138.
31. K. Huang, C.-L. Sun and Z.-J. Shi, *Chem. Soc. Rev.*, 2011, **40**, 2435-2452.
32. H. Yang, Z. Xu, M. Fan, R. Gupta, R. B. Slimane, A. E. Bland and I. Wright, *J. Environ. Sci.*, 2008, **20**, 14-27.
33. M. Mikkelsen, M. Jorgensen and F. C. Krebs, *Energ. Environ. Sci.*, 2010, **3**, 43-81.
34. G. W. F. A. Cotton, C. A. Murillo, M. Bochmann, *Advanced Inorganic Chemistry*, Wiley, New York, 6th edn., 1999.
35. C. S. Yeh, K. F. Willey, D. L. Robbins, J. S. Pilgrim and M. A. Duncan, *J. Chem. Phys.*, 1993, **98**, 1867-1875.
36. R. S. Walters, N. R. Brinkmann, H. F. Schaefer and M. A. Duncan, *J. Phys. Chem. A*, 2003, **107**, 7396-7405.
37. J. B. Jaeger, T. D. Jaeger, N. R. Brinkmann, H. F. Schaefer and M. A. Duncan, *Can. J. Chem.*, 2004, **82**, 934-946.
38. N. R. Walker, R. S. Walters and M. A. Duncan, *J. Chem. Phys.*, 2004, **120**, 10037-10045.
39. G. Gregoire and M. A. Duncan, *J. Chem. Phys.*, 2002, **117**, 2120-2130.
40. N. R. Walker, R. S. Walters, G. A. Grieves and M. A. Duncan, *J. Chem. Phys.*, 2004, **121**, 10498-10507.
41. R. L. Asher, D. Bellert, T. Buthelezi and P. J. Brucat, *Chem. Phys. Lett.*, 1994, **227**, 623-627.
42. H. Dossmann , C. Afonso, D. Lesage, J.-C. Tabet and E. Uggerud, *Angew. Chem. Int. Ed.*, 2012, **51**, 6938-6941.
43. G. B. S. Miller, T. K. Esser, H. Knorke, S. Gewinner, W. Schöllkopf, N. Heine, K. R. Asmis and E. Uggerud, *Angew. Chem. Int. Ed.*, 2014, **53**, 14407-14410.
44. G. B. S. Miller and E. Uggerud, *Chem. -- Eur. J.*, 2018, DOI: 10.1002/chem.201706069, 4710.
45. G. B. S. Miller and E. Uggerud, *Org. Biomol. Chem.*, 2017, **15**, 6813-6825.
46. M. J. Frisch, G. W. Trucks, H. B. Schlegel, G. E. Scuseria, M. A. Robb, J. R. Cheeseman, G. Scalmani, V. Barone, B. Mennucci, G. A. Petersson, H. Nakatsuji, M. Caricato, X. Li, H. P. Hratchian, A. F. Izmaylov, J. Bloino, G. Zheng, J. L. Sonnenberg, M. Hada, M. Ehara, K. Toyota, R. Fukuda, J. Hasegawa, M. Ishida, T. Nakajima, Y. Honda, O. Kitao, H. Nakai, T. Vreven, J. A. Montgomery Jr., J. E. Peralta, F. Ogliaro, M. J. Bearpark, J. Heyd, E. N. Brothers, K. N. Kudin, V. N. Staroverov, R. Kobayashi, J. Normand, K. Raghavachari, A. P. Rendell, J. C. Burant, S. S. Iyengar, J. Tomasi, M. Cossi, N. Rega, N. J. Millam, M. Klene, J. E. Knox, J. B. Cross, V. Bakken, C. Adamo, J. Jaramillo, R. Gomperts, R. E. Stratmann, O. Yazyev, A. J. Austin, R. Cammi, C. Pomelli, J. W. Ochterski, R. L. Martin, K. Morokuma, V. G. Zakrzewski, G. A. Voth, P. Salvador, J. J. Dannenberg, S. Dapprich, A. D. Daniels, Ö. Farkas, J. B. Foresman, J. V. Ortiz, J. Cioslowski and D. J. Fox, *Journal*, 2009.
47. P. J. K. H.-J. Werner, G. Knizia, F. R. Manby, M. Schütz, P. Celani, W. Györffy, D. Kats, T. Korona, R. Lindh, A. Mitrushenkov, G. Rauhut, K. R. Shamasundar, T. B. Adler, R. D. Amos, A. Bernhardsson, A. Berning, D. L. Cooper, M. J. O. Deegan, A. J. Dobbyn, F. Eckert, E. Goll, C. Hampel, A. Hesselmann, G. Hetzer, T. Hrenar, G. Jansen, C. Köppl, Y. Liu, A. W. Lloyd, R. A. Mata, A. J. May, S. J. McNicholas, W. Meyer, M. E. Mura, A. Nicklaß, D. P. O'Neill, P. Palmieri, D. Peng, K. Pflüger, R. Pitzer, M. Reiher, T. Shiozaki, H. Stoll, A. J. Stone, R. Tarroni, T. Thorsteinsson, M. Wang . , MOLPRO is a package of ab initio programs, https://www.molpro.net).
48. W. Hans-Joachim, K. P. J., K. Gerald, M. F. R. and S. Martin, *Wiley Interdisciplinary Reviews: Computational Molecular Science*, 2012, **2**, 242-253.
49. M. Bastian, S. Heymann and M. Jacomy, *Gephi: An Open Source Software for Exploring and Manipulating Networks*, 2009.
50. D. Tzeli and A. Mavridis, *J. Chem. Phys.*, 2008, **128**, 034309.
51. D. Tzeli, U. Miranda, I. G. Kaplan and A. Mavridis, *J. Chem. Phys.*, 2008, **129**, 154310.

52. A. J. Bridgeman and J. Rothery, *Journal of the Chemical Society, Dalton Transactions*, 2000, DOI: 10.1039/A906523G, 211-218.
53. K. Boguslawski, C. R. Jacob and M. Reiher, *J. Chem. Theory Comput.*, 2011, **7**, 2740-2752.
54. M. Reiher, *Chimia*, 2009, **63**, 140-145.
55. K. Pearson, *Notes on regression and inheritance in the case of two parents*, Royal Society, London, 1895.
56. S. Xantheas, S. T. Elbert and K. Ruedenberg, *J. Chem. Phys.*, 1990, **93**, 7519-7521.
57. S. S. Xantheas, G. J. Atchity, S. T. Elbert and K. Ruedenberg, *J. Chem. Phys.*, 1991, **94**, 8054-8069.
58. S. S. Xantheas and K. Ruedenberg, *Int. J. Quantum Chem.*, 1994, **49**, 409-427.
59. Y. Ma, L. Peng, H. Zhang and J.-G. Yu, *Russ. J. Phys. Chem. A*, 2014, **88**, 2339-2347.
60. T. Müller, S. S. Xantheas, H. Dachsel, R. J. Harrison, J. Nieplocha, R. Shepard, G. S. Kedziora and H. Lischka, *Chem. Phys. Lett.*, 1998, **293**, 72-80.
61. S. Kardahakis and A. Mavridis, *J. Phys. Chem. A*, 2009, **113**, 6818-6840.
62. D. Schröder, S. Bärsch and H. Schwarz, *Int. J. Mass Spectrom.*, 1999, **192**, 125-139.
63. L. G. Muzangwa, V. L. Ayles, S. Nyambo and S. A. Reid, *J. Mol. Spectrosc.*, 2011, **269**, 36-40.
64. A. J. Bridgeman, *Journal of the Chemical Society, Dalton Transactions*, 1997, DOI: 10.1039/A704478J, 4765-4772.
65. D. L. Hildenbrand, *J. Phys. Chem. A*, 2008, **112**, 3813-3815.